2-1-2004

High-Quality, Melt-Grown ZnO Single Crystals

D. C. Reynolds

C. W. Litton

David C. Look
Wright State University - Main Campus, david.look@wright.edu

J. E. Joelscher

B. Claflin

See next page for additional authors

High-quality, melt-grown ZnO single crystals

D. C. Reynolds and C. W. Litton[a)]
Materials and Manufacturing Directorate, Air Force Research Laboratory, AFRL/MLPS, Wright-Patterson Air Force Base, Ohio 45433

D. C. Look, J. E. Hoelscher, and B. Claflin
Semiconductor Research Center, Wright State University, Dayton, Ohio 45435 and Air Force Research Laboratory, AFRL/MLPS, Wright-Patterson Air Force Base, Ohio 45433

T. C. Collins
Oklahoma State University, 203 Whitehurst Hall, Stillwater, Oklahoma 74078

J. Nause and B. Nemeth
Cermet, Inc., 1019 Collier Road, Atlanta, Georgia 30318

(Received 25 November 2003; accepted 10 February 2004)

High-quality, melt-grown ZnO crystals are reported. The reflection and emission spectra of the melt-grown samples are compared with the same spectra from high-quality, vapor-grown ZnO crystals. We isolate the reflection and emission spectra predominantly related to the intrinsic properties associated with the wurtzite structure of the crystals. The quality of the crystals is reflected in the spectral reproduction of the intrinsic properties of the crystals. Both the ground state and the $n=2$ state of the free excitons associated with the A, B, and C valence bands of the crystals are spectrally observed in reflection. Assuming a hydrogenic character for the free excitons, the binding energy of these excitons associated with all three valence bands was determined. For the intrinsic emission spectra, attention was focused on the A-band free excitons and related optical parameters. Both the reflection and emission spectra for the melt-grown material compared very closely with the same spectra observed from high-quality vapor-grown ZnO samples. The details of both the reflection and emission spectra verify the high-quality of the melt-grown material. [DOI: 10.1063/1.1691186]

INTRODUCTION

Zinc oxide (ZnO) is a wide-bandgap semiconductor which has great potential for both electronic and optoelectronic devices. Some ZnO properties that support this assertion are (a) low threshold power for optical pumping of bandgap lasing at room temperature,[1–3] (b) a large free exciton binding energy (~60 meV), which may give rise to efficient UV lasing at room temperature, and (c) a tunable bandgap which occurs when ZnO is alloyed with CdO and MgO to form thin films of the ternary alloys $Cd_yZn_{1-y}O$ and $Mg_xZn_{1-x}O$, whose bandgaps can be reduced down to ~2.8 eV and increased up to ~4.0 eV, respectively.[4–8] The bandgap of the $Mg_xZn_{1-x}O$ alloy system can also be varied through growth and formation of $Mg_xZn_{1-x}O$/ZnO quantum well heterostrutures[9,10] and superlattices.[11,12] To achieve these potential applications, high-quality single-crystal substrates will be required. High-quality ZnO crystals have been grown by the vapor phase[13] and hydrothermal methods.[14] Rather recently, high-quality crystals have been grown by a pressurized melt-growth technique.[15] This method can also produce large size, large diameter, single-crystal boules, which makes them also useful for substrate applications. The unique properties of ZnO combined with the capability of growing high-quality single crystals in bulk form establishes it as a leading wide-bandgap semiconductor for many commercial device applications.

EXPERIMENTAL DETAILS

The high-quality melt-grown samples were grown at Cermet, Inc., Atlanta, GA, using a pressurized melt growth process. This approach utilizes a patented method of melting and crystallizing materials that have high melting point (particularly above ~1450 °C), a volatile component in the structure, or thermodynamic instabilities at or near the material's melting point (decomposes into atomic components) at atmospheric pressure. The technique uses a high-pressure induction melting apparatus, wherein the melt is contained in a water-cooled crucible.

The heat source used during the melting operation is rf energy. Induced fields in the crystalline charge material (powder) produce eddy currents, which produce Joule heating in the material until a molten phase is achieved. The highly refractory melt produced is contained in a cold-wall crucible, such that part of the solid thermal barrier between the molten material and the cooling fluid is cooled material with the same composition as the melt. The cooled material prevents the molten material from coming into direct contact with the cooling surface, which eliminates containment problems and crucible reactivity regardless of the melting temperature of the material. This entire melting and containment

a)Author to whom correspondence should be addressed; electronic mail: cole.litton@wpafb.af.mil

process is carried out in a controlled gas atmosphere ranging from 1 to over 100 atmospheres, which prevents the evolution of volatile components, as well as the decomposition of some compounds into atomic species. The system has been proven at temperatures in excess of 3600 °C and melt environments in excess of 100 atmospheres. For example, the system has been used to melt and solidify aluminum nitride (AlN).

In standard melt-growth atmospheres, ZnO decomposes upon heating into a highly defective ZnO_{1-x} structure. This problem has been overcome by providing an overpressure of oxygen as the growth atmosphere. A thermodynamic equilibrium between the liquid ZnO and the oxygen reservoir is established, thereby preventing reduction of the lattice. The stoichiometric ZnO melt is contained in a thin layer of cooled polycrystalline ZnO, which eliminates crucible-introduced impurities. The process, which is ultimately scalable to large dimensions, has been used to melt 5.5-inch-diameter, kilogram sized ingots of ZnO.

For optical measurements, the crystal was mounted on a copper holder with its *c* axis oriented parallel to the long dimension of the rectangular holder. This was contained in the vacuum chamber of a variable-temperature dewar. The reflectivity spectral measurements were made at 5 K using a high-pressure Xe arc lamp, which provided ample continuum in the UV spectral region of interest. Photoluminescence (PL) spectral measurements were made with the same dewar at 5 K. PL excitation was achieved with the 3250 Å line of a HeCd laser. Both the high-resolution PL and reflectivity spectra were analyzed with a 4 m grating spectrometer, using a RCAC31034 photomultiplier for detection.

EXPERIMENTAL RESULTS

We emphasize the high-quality of the currently investigated, melt-grown ZnO crystals,[15] by comparing their reflection spectra with the same spectra measured on high-quality, vapor-grown ZnO.[13] The reflection spectra are predominantly sensitive to the intrinsic properties of the crystals, and not their extrinsic properties, such as impurity states. The details of the intrinsic band structure and its interaction with radiation can be described as follows. The dipole moment operator for electronic dipole radiation transforms like *x*, *y*, or *z*, depending on the polarization. When the electric vector **E** of the incident light is parallel to the crystalline *c* axis, the operator corresponds to the Γ_1 representation. When it is perpendicular to the *c* axis, the operator corresponds to the Γ_5 representation. Since ZnO is of the wurtzite crystal structure, it has a principal axis, the *c* axis, and as a result, the crystal field lifts part of the degeneracy of the P levels of the valence band. Thus, disregarding spin–orbit coupling, the following decomposition at the center of the Brillouin zone is obtained:

$$\text{Conduction band: } S \rightarrow \Gamma_1,$$

$$P_x, P_y \rightarrow \Gamma_5,$$

$$\text{Valence band: } P_z \rightarrow \Gamma_1.$$

This is shown in Fig. 1(a).

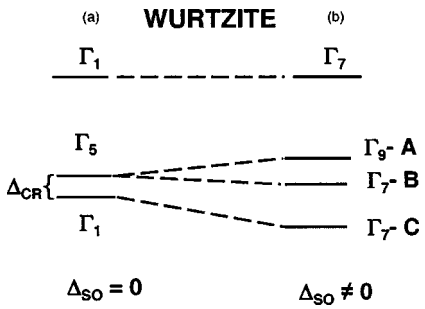

FIG. 1. Energy band structure of wurtzite ZnO, showing the conduction and valence band symmetries and degeneracies at the zone center: (a) in the absence of and (b) in the presence of spin–orbit coupling.

Introduction of spin doubles the number of levels. The splitting caused by the presence of spin is represented by the inner products

$$\Gamma_5 \times D_{1/2} \rightarrow \Gamma_7 + \Gamma_9,$$

$$\Gamma_1 \times D_{1/2} \rightarrow \Gamma_7,$$

and the band structure at $\mathbf{K}=0$, when spin is included, along with the symmetries, is shown in Fig. 1(b). The details of the measured intrinsic properties are a good measure of the crystal quality of the samples. In Fig. 2, we show the reflection spectrum from a high-quality vapor-grown sample (dashed curve) with that of a melt-grown sample (solid curve). These spectra were measured in the orientation, $\mathbf{E}\perp\mathbf{c}$, which minimizes the C band. In both the vapor-grown and melt-grown samples, the A and B bands can be observed. In addition, a structure at A′ and B′ is observed. The polarization properties of A′ and B′ indicate that they are associated with the transitions A and B, respectively. The A and B transitions correspond to the ground state transitions associated with the first and second valence bands, respectively. The weaker transitions A′ and B′ result from the $n=2$ states of the parent transitions. Assuming that the excitons are hydrogen-like, an estimate of their binding energies can be made. We should note that the energy band details are reflected in both the

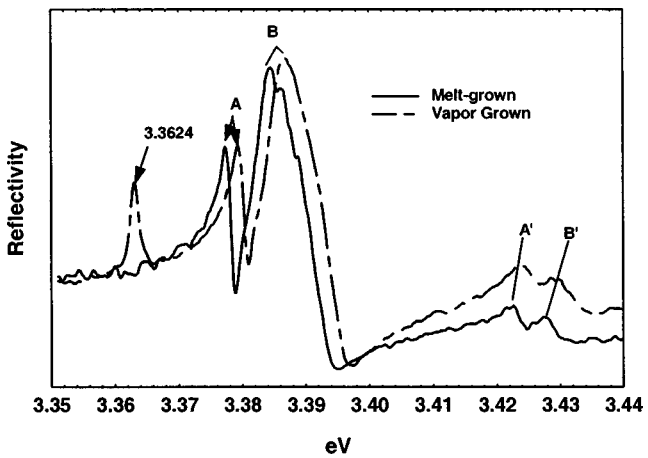

FIG. 2. Reflection spectra, measured in the polarization, $\mathbf{E}\perp\mathbf{c}$, from a high-quality vapor-grown crystal (dashed curve) and from a melt-grown crystal (solid curve). The $n=2$ transitions, A′ and B′, from the A and B bands of both samples are observed.

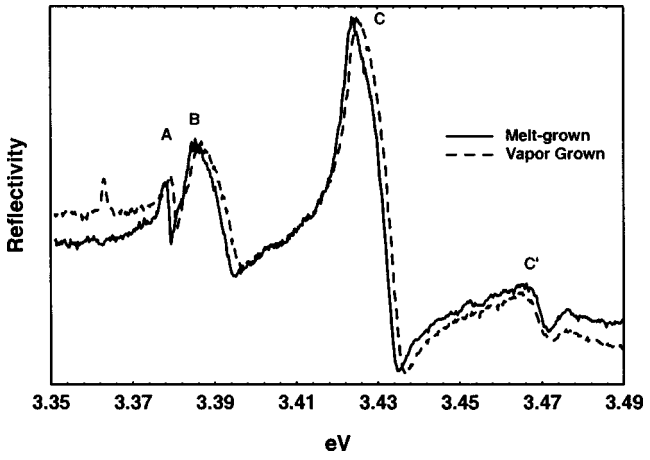

FIG. 3. Reflection spectra showing transitions from the A, B, and C bands from both vapor-grown (dashed curve) and melt-grown (solid curve) samples are illustrated here. Transitions from the $n=2$ state of the C band (C') in both samples are also observed.

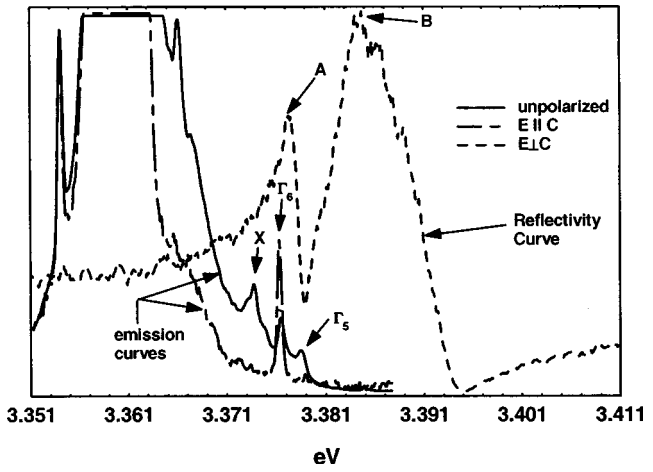

FIG. 4. Emission spectra from a melt-grown sample, emphasizing the intrinsic exciton transitions associated with the A band and with the Γ_5 and Γ_6 and X (polariton) states. The emission is both unpolarized (solid curve) and polarized, $\mathbf{E}\|\mathbf{c}$ (dashed curve), showing the transverse character of both Γ_5 and X. A reflection spectrum, polarized with $\mathbf{E}\perp\mathbf{c}$, is also shown.

vapor-grown and the melt-grown samples, showing the high quality of both types of samples. In Fig. 3, the reflection spectra of both samples are shown in unpolarized light. Here, in addition to the A and B bands, the C band as well as C' are observed. The dashed curve is the spectrum for the vapor-grown sample, while the solid curve is for the melt-grown sample. As was the case for the A and B bands, C is the ground state transition for the third valence band. As with the A and B bands, C' is the $n=2$ state of the ground state transition. It should be noted in both Figs. 2 and 3 that a transition at 3.3624 eV is observed in the vapor-grown sample, but not in the melt-grown sample. This transition has been reported[16] to be due to a hydrogen impurity. The difference in the growth processes, previously discussed, explains why hydrogen would not be present in the melt-grown process, but gaseous hydrogen is known to be present at high concentrations in the vapor transport growth process.

As previously mentioned, if one assumes that the excitons are hydrogenic, then the exciton binding energies can be obtained from the energies of their ground and excited states. These energies are given in Table I and are compared with the same energies reported by Thomas[17] measured on hexagonal needles grown from the vapor phase. It is observed that there is good agreement, within experimental error, for the three different growth techniques.

We have also observed, in the melt-grown sample, the intrinsic excitons associated with the A band in emission spectra, shown in Fig. 4. The Γ_5 and Γ_6 excitons are well resolved and an additional transition, denoted as X, is also observed. This transition is believed to be associated with the lower polariton branch of the A exciton (LPB_A), and is discussed more fully in Ref. 18. The three emissive transitions, Γ_5, Γ_6, and X, can be compared with the same three transitions reported for vapor-grown material, and are shown as Fig. 3 in Ref. 18. When the polarizer is positioned at $\mathbf{E}\|\mathbf{c}$, both Γ_5 and X are very much diminished, both having transverse properties, and the Γ_6, which has longitudinal properties, is very much enhanced. Therefore, X must be associated with the LPB_A except that it must occur at the lower $\mathbf{K}$ value, since it has a lower energy. It is likely that X is in the ''bottleneck'' region, that is, the region in which the photon and free-exciton dispersion curves cross over.

Hall-effect measurements were carried out on typical melt-grown ZnO samples, using Accent HL 5500PC (room temperature) and LakeShore 7507 variable temperature systems. The room-temperature results were as follows: samples were *n*-type with a typical resistivity of 0.49 Ω cm, a typical mobility of 150 $cm^2/V\,s$ and a typical electron concentration of 8.4×10^{16} cm^{-3}. These parameters compare favorably with those found for the pure, vapor-phase-grown (VP) material,[19] although the mobility is somewhat lower. Variable temperature (20–340 K) mobility and carrier concentration data were fitted with models described elsewhere,[19] and yield

TABLE I. Spectral positions and binding energies of free excitons in ZnO.

Excitonic oscillator	Spectral position (vapor grown) (eV)	Spectral position (melt grown) (eV)	Spectral position (hexagonal needle) (eV)	Free exciton binding energy (meV)		
				Vapor	Melt	Needle
A	3.3783	3.3764	3.3768	59.5	60.4	60.9
A′	3.4229	3.4217	3.4225			
B	3.3858	3.3840	3.383	56.6	57.5	59.3
B′	3.4283	3.4271	3.4275			
C	3.4245	3.4336	3.4215	56.3	56.1	58.0
C′	3.4667	3.4657	3.465			

the following parameters: $N_D = 1.5 \times 10^{17}$ cm^{-3}; donor activation energy $E_D = 26$ meV; and acceptor concentration $N_A = 2.7 \times 10^{16}$ cm^{-3}. Here, N_D is about the same as that found for the VP material, and N_A is about an order of magnitude higher. If the dominant acceptor for the present melt-grown ZnO is the Zn vacancy, as is known to be the case for the VP material,[20] then the O/Zn stoichiometry ratio may be higher for the melt-grown ZnO. It is already known, for example, that the melt-grown ZnO crystals employed in the present study were grown under a high oxygen overpressure, as discussed earlier under experimental growth conditions.

CONCLUSIONS

We can conclude from the reflection and emission spectral data, as well as the Hall transport measurements, that the melt-grown crystals of ZnO are comparable in quality to the vapor-grown crystals, which we know to be of very high quality from many other fundamental measurements of their optical and electrical properties and parameters.

ACKNOWLEDGMENTS

We wish to thank Z-Q. Fang for helpful discussions and T. A. Cooper and W. Rice for technical assistance. Two authors (D. C. R. and C. W. L.) were supported under AFOSR Lab Task 2305EL, managed by Lt. Col. Todd Steiner (PhD), while three authors (D. C. L., J. E. H. and B. C.) were supported by U. S. Air Force Contract F33615-00-C-5402.

[1] M. Kawasaki, A. Ohtomo, I. Ohkubu, H. Koinuma, Z. K. Tang, P. Yu, G. K. L. Wong, B. P. Zhang, and Y. Segawa, Mater. Sci. Eng., B **56**, 239 (1998).
[2] D. M. Bagnall, Y. F. Chen, Z. Zhu, T. Yao, S. Koyama, M. Y. Chen, and T. Goto, Appl. Phys. Lett. **70**, 2230 (1997).
[3] Z. K. Yang, P. Yu, G. K. L. Wong, M. Kawasaki, A. Ohtomo, H. Koinuma, and Y. Segawa, Solid State Commun. **103**, 459 (1997).
[4] A. Ohtomo, M. Kawasaki, T. Koida, K. Masabuchi, H. Koinuma, Y. Sakurai, Y. Yoshida, T. Yasuda, and Y. Segawa, Appl. Phys. Lett. **72**, 2466 (1998).
[5] A. K. Sharma, J. Narayan, J. F. Muth, C. W. Teng, C. Jin, A. Kvit, R. M. Kolvas, and O. W. Holland, Appl. Phys. Lett. **75**, 3327 (1999).
[6] T. Minemoto, T. Negami, S. Nishiwaki, H. Takakura, and Y. Hamakawa, Thin Solid Films **372**, 173 (2000).
[7] W. I. Park, G. Yi, and H. M. Yang, Appl. Phys. Lett. **79**, 2022 (2001).
[8] T. Makino, Y. Segawa, M. Kawasaki, A. Ohtomo, R. Shiroki, K. Tamura, T. Yasuda, and H. Koinuma, Appl. Phys. Lett. **78**, 1237 (2001).
[9] D. Sun, T. Makino, N. T. Tuan, Y. Segawa, Z. K. Tang, G. K. L. Wong, M. Kawasaki, A. Ohtomo, K. Tamura, and H. Koinuma, Appl. Phys. Lett. **77**, 4250 (2000).
[10] D. Sun, T. Makino, Y. Segawa, M. Kawasaki, A. Ohtomo, K. Tamura, and H. Koinuma, J. Appl. Phys. **91**, 1993 (2002).
[11] A. Ohtomo, M. Kawasaki, I. Ohkubo, H. Koinuma, T. Yasuda, and Y. Segawa, Appl. Phys. Lett. **75**, 980 (1999).
[12] A. Ohtomo, K. Tamura, M. Kawaski, T. Makino, Y. Segawa, Z. K. Tang, G. K. L. Wong, Y. Matsumoto, and H. Koinuma, Appl. Phys. Lett. **77**, 2204 (2000).
[13] G. Cantwell and D. B. Eason, in *Properties, Processes and Applications of ZnO*, edited by C. W. Litton, D. C. Reynolds, and T. C. Collins (IEE IOP, London, 2004), Chap. 6 (in press).
[14] K. Byrappa and M. Yoshimura, in *Handbook of Hydrothermal Technology* (William Andrew, New York, 2001) Chaps. 1–5; see also M. J. Callahan, D. F. Bliss, M. T. Harris, and M. N. Alexander, in *Properties, Processes and Applications of ZnO*, edited by C. W. Litton, D. C. Reynolds and T. C. Collins (IEE IOP, London, 2004), Chap. 8 (in press).
[15] J. Nause and B. Nemeth, in *Properties, Processes and Applications of ZnO*, edited by C. W. Litton, D. C. Reynolds, and T. C. Collins (IEE IOP, London, 2004), Chap. 7 (in press).
[16] Y. M. Strzhemechny, J. Nemergut, P. E. Smith, J. Bae, D. C. Look, and L. J. Brillson, J. Appl. Phys. **94**, 4256 (2003).
[17] D. G. Thomas, Phys. Chem. Solids **15**, 86 (1960).
[18] D. C. Reynolds, D. C. Look, B. Jogai, and T. C. Collins, Appl. Phys. Lett. **79**, 3794 (2001).
[19] D. C. Look, D. C. Reynolds, J. R. Sizelove, R. L. Jones, C. W. Litton, G. Cantwell, and W. C. Harsch, Solid State Commun. **105**, 399 (1998).
[20] F. Tuomisto, V. Ranki, K. Saarinen, and D. C. Look, Phys. Rev. Lett. **91**, 205502 (2003).